Manuscript prepared for J. Name
with version 4.2 of the LaTeX class copernicus.cls.
Date: 10 May 2015

# Strong aerosol-cloud interaction in altocumulus during updraft periods: lidar observations over central Europe

**J. Schmidt, A. Ansmann, J. Bühl, and U. Wandinger**

Leibniz Institute for Tropospheric Research, Leipzig, Germany

**Abstract.** For the first time, a detailed lidar-based study of the aerosol-cloud-dynamics relationship was conducted. Twenty nine cases of pure liquid-water altocumulus layers were observed with a novel dual-field-of-view (dual-FOV) Raman lidar over the polluted central European site of Leipzig, Germany, between September 2010 and September 2012. By means of the novel Raman lidar technique cloud properties such as the droplet effective radius and cloud droplet number concentration (CDNC) in the lower part of altocumulus layers are obtained. The conventional aerosol Raman lidar technique provides the aerosol extinction coefficient (used as aerosol proxy) below cloud base. A collocated Doppler lidar measures the vertical velocity at cloud base and thus updraft and downdraft occurrence. Here, we present the key results of our statistical analysis of the 2010–2012 observations. Besides a clear aerosol effect on cloud droplet number concentration in the lower part of the altocumulus layers during updraft periods, turbulent mixing and entrainment of dry air is assumed to be the main reason for the found weak correlation between aerosol proxy and CDNC higher up in the cloud. The corresponding aerosol-cloud interaction (ACI) parameter based on changes in cloud droplet number concentration with aerosol loading was found to be close to 0.8 at 30–70 m above cloud base during updraft periods and below 0.4 when ignoring vertical-wind information in the analysis. Our findings are extensively compared with literature values and agree well with airborne observations.

## 1 Introduction

The indirect aerosol effect on climate results from two cloud-influencing aspects. Atmospheric aerosol particles act as cloud condensation nuclei (CCN) in liquid-water droplet formation and as ice nuclei (IN) in processes of heterogeneous ice nucleation. There is no doubt that aerosols play a key role in the evolution of warm (pure liquid-water) and mixed-phase clouds and in the formation of precipitation and that anthropogenic and natural aerosols thus sensitively influence the atmospheric water cycle as a whole. Aerosol-cloud interaction (ACI) at given meteorological conditions must be well understood and properly parameterized in atmospheric circulation models to improve future climate predictions. The models must be able to handle all natural and man-made aerosol types from the emission over regional and long-range transport to deposition and the interaction of the different aerosols with clouds. However, we are far away from a good representation of aerosols and their complex role in the climate system in computer models, especially with respect to aerosol vertical layering so that the uncertainties in climate predictions remain very high.

**We need strong efforts of continuous, long-term observations of aerosols and clouds around the globe by means of active remote sensing with cloud radar and aerosol/cloud lidar (Shupe, 2007) at well-equipped super sites such as the Atmospheric Radiation Measurment (ARM) sites in Oklahoma (Feingold et al., 2006; Ferrare et al., 2006) and tropical Australia (Riihimaki et al., 2012) and the ARM Mobile Facility to overcome this unsatisfactory situation.** We further need well-coordinated ground-based networks such as CLOUDNET (Illingworth et al., 2007) and, complementary, also observations from space (Bühl et al., 2013). CLOUDNET may be regarded as a prototype network for the development of ground-based aerosol and cloud monitoring infrastructures. Continuous detection of all aerosol layers and embedded warm, mixed-phase, and ice clouds with high vertical and temporal resolution is required. In addition, measurements of vertical movements (updrafts, downdrafts, gravity waves) are demanded because vertical motions control all cloud processes (Twomey, 1959; Ghan et al., 1993, 1997, 2011; Morales and Nenes, 2010). New tech-

*Correspondence to:* A. Ansmann (albert@tropos.de)

niques as well as new combinations of existing techniques and tools need to be introduced to improve our ability to study ACI in the necessary detail and to provide in this way fundamental, reliable information for the improvement of cloud parameterization schemes in cloud-resolving models.

In the framework of a feasibility study from 2008–2012, we investigated the potential of a novel cloud lidar (Schmidt et al., 2013; Schmidt, 2014) combined with a Doppler lidar for vertical wind profiling to provide new insight into the influence of aerosol particles on the evolution of pure liquid-water altocumulus layers (Schmidt et al., 2014). These clouds are usually optically thin enough so that lidar can provide information on cloud optical and microphysical properties and up- and downdraft characteristics throughout the cloud layer from base to top.

The novel dual-field-of-view (dual-FOV) Raman lidar allows us to measure aerosol particle extinction coefficients (used as aerosol proxy) close to cloud base and to retrieve cloud microphysical properties such as cloud droplet effective radius $r_{\mathrm{e}}$ and cloud droplet number concentration (CDNC) in the lower part of the cloud. The development of this novel lidar technique was motivated by numerous published ACI studies (see Sect. 4), in which aerosol observations (at ground or far below cloud base) were correlated with remote-sensing products such as the cloud-column-averaged effective radius or cloud mean droplet number concentration to describe the impact of a given aerosol load on the evolution and microphysical properties of a cloud layer. To our opinion, such experimental approaches do not allow an accurate quantification of ACI. We will discuss this issue in detail in Sect. 4.

**To significantly contribute to the field of aerosol-cloud-interaction research, a large number of observations are required to produce statistically significant constraints on sub-grid scale cloud parameterizations used in weather and climate models. Many of these parameterizations are developed on the basis of a few cases studies. However, even after three years of cloud lidar observations, this remains a difficult task. We sampled more than 200 stratocumulus and altocumulus layers (liquid and mixed-phase stratiform cloud layers) within the main observational period from September 2010 to September 2012, but only 29 non-drizzeling purely liquid-water cloud layers (mainly altocumulus) remained finally for the statistical analysis presented in Sect. 3. Only 13 of such cloud cases (out of about 100 cases) were measured with the combined dual FOV and Doppler lidar facility. Nevertheless, based on this small aerosol/cloud data set, several clear conclusion can be drawn and are presented in Sects. 3 and 4. We will continue with our observations during the next years to improve the statistical data base significantly.**

Schmidt et al. (2014) already presented several case studies of combined dual-FOV Raman lidar and Doppler lidar observations in shallow cloud layers occurring over the polluted continental European site of Leipzig, Germany, in the lower free troposphere between 2.5 and 4 $\mathrm{km}$ height. Cases with clouds in clean and polluted aerosol environments were contrasted. The importance of Doppler lidar observations of the updraft and downdraft conditions at cloud base was highlighted. Here, we extend this discussion and summarize our multi-year observations. We present the main results of the statistical analysis of the 29 cloud cases. Because lidar profiling through water clouds from bottom to top is only possible up to cloud optical depths of 3.0 and respective liquid water paths (LWPs) of up to about 50 $\mathrm{g\,m^{-2}}$ our statistics covers thin altocumulus clouds only. Nevertheless, the message of the paper is clear: only during updraft periods an unambiguous and strong relationship between aerosol burden and cloud microphysical properties is observed. This is the main topic of the paper and will be discussed in Sect. 3.

We begin with a brief description of the remote sensing instrumentation in Sect 2. Definitions of well-established aerosol-cloud interaction parameters are given in the Sect. 2, too. Section 3 discusses the experimental findings in terms of ACI statistics, and Sect. 4 provides an extended comparison of ACI literature values. A summary and concluding remarks are given in Sect. 5.

## 2 Lidar instrumentation and ACI parameters

In 2011, the Leipzig Aerosol and Cloud Remote Observation System (LACROS, 51.3° N, 12.4° E) (Wandinger et al., 2012; Schmidt et al., 2014) of the Leibniz Institute for Tropospheric Research (TROPOS), Leipzig, Germany, was established. The major tools of LACROS are a multiwavelength Raman/polarization lidar which is part of EARLINET (European Aerosol Research Lidar Network) (Pappalardo et al., 2014), a wind Doppler lidar, a 35 GHz cloud radar, a microwave radiometer, as well as an Aerosol Robotic Network (AERONET) sun/sky photometer (Holben et al., 1998). LACROS belongs to the CLOUDNET consortium. The Raman lidar was upgraded to perform dual-FOV Raman lidar measurements for the retrieval of cloud microphysical properties in 2008 (Schmidt et al., 2013). The laser transmits wavelengths at 355, 532, and 1064 nm.

The novel cloud lidar technique (Schmidt et al., 2013, 2014; Schmidt, 2014) makes use of two receiver FOVs. Raman scattered light with a wavelength of 607 nm is detected with a conventional, circular FOV as well as with an annular, outer FOV encompassing the inner, circular FOV. The measurement geometry is illustrated in Fig. 1 in Schmidt et al. (2014). In the case of lidar measurements in clouds, multiply scattered light is detected in the outr FOV due to the pronounced forward scattering peak of the phase function of cloud droplets. The width of the forward scattering peak and thus the strength of the signal detected by the outer-FOV channel correlates unambiguously with the size of the scattering droplets. To be capable of performing dual-FOV

cloud measurements in an extended altitude range from 1.3 to 6 km height, the receiver of the dual-FOV Raman lidar is set up in the way that the measurement geometry can be easily optimized regarding the contrast of the multiple scattering effects in the two channels by exchanging the field stop (Schmidt et al., 2013). FOV pairs of 0.28 and 0.78 mrad (for clouds above about 4 km height), of 0.5 and 2.0 mrad (for clouds from about 2.7 to 4 km height) and of 0.78 and 3.8 mrad (for clouds with base <2.7 km) are used (Schmidt et al., 2013). Due to the small Raman scattering cross section, the dual-FOV Raman lidar measurements are restricted to nighttime hours.

The lidar permits us to characterize warm clouds (no ice phase) in terms of height profiles of single-scattering droplet extinction coefficient $\alpha$, cloud droplet number concentration $N$ (or CDNC), droplet effective radius $r_\mathrm{e}$, and liquid water content LWC (Schmidt et al., 2013, 2014). Since implemented in a conventional aerosol Raman lidar, detailed information of aerosol properties below cloud base are available in addition. We use the aerosol particle extinction coefficient $\alpha_\mathrm{p}$ measured at 532 nm as aerosol proxy.

**Table 1 provides an overview of the vertical and temporal resolution of the basic lidar measurements with the dual-FOV Raman lidar. Given are also the typical signal averaging and signal smoothing lengths, and a list of the retrieved aerosol and cloud products as well as the typical relative uncertainties of the retrieved quantities, caused by signal noise and the input parameters required in the retrieval procedure. The error analysis for the cloud extinction coefficient $\alpha$ and the cloud droplet effective radius $r_\mathrm{e}$ is described by Schmidt et al. (2013). The uncertainty in the cloud droplet number concentration, CDNC, is obtained from Eq. (4) in Schmidt et al. (2014) by applying the law of error propagation. CDNC is a function of $\alpha/r_\mathrm{e}^{-2}$ and thus the uncertainty of CDNC sensitively depends on the uncertainty in $r_\mathrm{e}$.**

**The Doppler wind lidar WILI of TROPOS operates at a wavelength of 2022 nm. Vertical and temporal resolutions are 70 m and 2 s, respectively. The uncertainty in the determination of the vertical–wind component is of the order of 10 cm/s. The Doppler lidar observations were used in our study to separate regions with upward and downward motions at cloud base (first and lowest height bin influenced by cloud backscatter). Our experience shows that the updrafts usually extend from the base to the top of the shallow stratiform cloud layers. The updraft strength may vary with height. To remotely sense the same volume with the Doppler and Raman lidars, both systems were located within a distance of less than 10 m and both lidars were pointing exactly to the zenith.**

**The cloud radar of LACROS is used here only for drizzle detection and cloud top identification to corroborate the lidar observations in cases with optically dense clouds. However, in most cases, periods with reduced clouds optical thickness occurred when the shallow cloud layers crossed the lidar site so that cloud top height was usually obtained from the lidar observations. The HATPRO microwave radiometer were used to estimate LWP which can be compared with the column–integrated liquid water content (LWC) obtained from the dual–FOV Raman lidar observations (as explained in the next section).**

To better quantify the aerosol effect on cloud properties (in Sect. 3) and to better compare our results with literature values (in Sect. 4), we computed two well-established ACI parameters (Feingold et al., 2001; Garrett et al., 2004; McComiskey and Feingold, 2008; McComiskey et al., 2009).

The nucleation-efficiency parameter is defined as:

$$\mathrm{ACI_N} = \mathrm{d}\ln(N)/\mathrm{d}\ln(\alpha_\mathrm{p}) \quad (1)$$

with the cloud droplet number concentration $N$ and the aerosol particle extinction coefficient $\alpha_\mathrm{p}$. $\mathrm{ACI_N}$ describes the relative change of the droplet number concentration with a relative change in the aerosol loading.

The indirect-effect parameter $\mathrm{ACI_r}$ is defined as:

$$\mathrm{ACI_r} = -\partial\ln(r_\mathrm{e})/\partial\ln(\alpha_\mathrm{p}). \quad (2)$$

$\mathrm{ACI_r}$ describes the relative change of the droplet effective radius $r_\mathrm{e}$ with a relative change in the aerosol extinction coefficient $\alpha_\mathrm{p}$ at constant LWP (or LWC) conditions. $\mathrm{ACI_r}$ is equal to 1/3 $\mathrm{ACI_N}$ (for constant LWP) according to the $r_\mathrm{e} \propto N^{-1/3}$ relationship. More details can be found in Schmidt et al. (2014).

Figure 1 illustrates how we tried to link aerosol properties with cloud properties. As aerosol proxy we used the particle extinction coefficient $\alpha_\mathrm{p}$ for the layer from 300–1000 m below the lowermost cloud base height. These 532 nm extinction coefficients were obtained by means of the Raman lidar method. A distance of 300 m to the cloud layer base was usually sufficient to avoid that particle water-uptake effects influenced $\alpha_\mathrm{p}$. Water uptake occurs when the relative humidity increases from values below about 60 % towards 100 % at cloud base (see examples in Schmidt et al., 2014). As cloud properties we selected CDNC and droplet effective radius for distinct layers from 0–30 m, 30–70 m, and 70–120 m above the lowest detected cloud base.

**To reduce signal noise the basic lidar signal profiles (obtained and stored with 10 s resolution) were averaged over 10–90 minutes, depending on the homogeneity and lifetime of the observed cloud layers. We selected only cloud layers with well-defined temporally almost constant cloud base height and homogeneous cloud backscatter structures for our study. When averaging lidar signal profiles, the lowermost cloud base height occurring during the averaging time interval (and not the mean cloud base height) shows up as cloud base height in the averaged signal profile, as illustrated in Fig. 1.**

## 3 Statistical analysis

### 3.1 Overview of aerosol and cloud properties

**During this 2008-2012 feasibility study, the dual-FOV lidar was run manually (not in an automated mode) to always allow a careful alignment of the new lidar receiver setup, especially an optimum selection of the two FOVs for a given cloud layer height range. The lidar was operated only when atmospheric conditions were favorable. The measurements were typically conducted during the first four hours after sunset. This is the main reason for the comparably low number of cloud cases we sampled during the 2-year period (2010-2012), after the test phase in 2008-2009.**

**All in all, we measured 200 stratiform cloud layers with the Raman lidar, 140 of these cloud layers were simultaneously observed with the cloud radar, and 100 of these cloud cases were simultaneously monitored with the Doppler lidar WILI. By using the polarization lidar technique (also implemented in the aerosol/cloud Raman lidar) for the identification of ice crystals (ice virga below cloud base), we first removed all mixed-phase clouds from the data set. We further eliminated all cases with strongly varying cloud backscatter properties including a strongly varying cloud base. Finally, 29 pure liquid-water cloud layers remained, of which 13 were measured together with Doppler lidar. Thus, to study explicitly the impact of updrafts on the strength of aerosol-cloud interaction, 13 cloud layers are available. Three of the 29 clouds occurred during pure updraft periods, 26 cloud layers showed updraft as well as downdraft influences.**

Table 2 summarized the main aerosol and cloud properties of the 29 aerosol/cloud cases observed from September 2010 to September 2012. All investigated 29 liquid clouds were geometrically and optically thin. The derived $532\,\mathrm{nm}$ aerosol particle extinction coefficients below cloud base ranged from 7–$130\,\mathrm{Mm^{-1}}$ with a mean value of $52 \pm 34\,\mathrm{Mm^{-1}}$. These aerosol conditions match well with findings of Mattis et al. (2004) who presented aerosol lidar results for the boundary layer and lower free troposphere over the EARLINET station at Leipzig between 2000 and 2003. Base heights and vertical extend of the observed cloud layers ranged from about 1–4.5 km and 100–300 m, respectively. Most clouds occurred in the free troposphere around $3 \pm 1$ km height. Table 3 summaries the cloud products derived from the dual-FOV Raman lidar observations. Most effective cloud droplet radii were found in the range from 5–$10\,\mu\mathrm{m}$ and CDNCs showed typical values from 50–$200\,\mathrm{cm^{-3}}$.

### 3.2 Lidar-derived $\mathrm{ACI_r}$ and $\mathrm{ACI_N}$ without considering vertical-wind information

Figure 2 shows a first overview of our lidar-based ACI studies. For the 26 cloud layers (with updraft and downdraft periods) the correlation between the cloud droplet effective radius in the cloud layer from 30–$70\,\mathrm{m}$ above cloud base and the aerosol particle extinction coefficient $\alpha_\mathrm{p}$ below cloud base is shown. Vertical wind information is not taken into account in this figure, i.e., the presented findings are based on lidar signal averages without any sorting of signals to updraft or downdraft periods.

As can be seen, the computed $\mathrm{ACI_r}$ values for two groups of LWC ranges are small. The $\mathrm{ACI_r}$ values are $0.10 \pm 0.17$ and $-0.01 \pm 0.09$ for the lower and higher LWCs cloud groups, respectively. The overall mean value of $\mathrm{ACI_r}$ value is $0.04 \pm 0.09$. The coefficients of determination $R^2$ from the linear regression of the $\mathrm{ACI_r}$ calculation are 0.03 and $< 0.01$ for the data set with the lower and higher LWC, respectively.

Figure 3 shows the correlation between CDNC and $\alpha_\mathrm{p}$ for the 26 dual-FOV Raman lidar measurements. On average, higher CDNCs are found for larger particle extinction coefficients. This tendency is expressed in an $\mathrm{ACI_N}$ value of $0.32 \pm 0.19$. The coefficient of determination obtained from the linear regression for the calculation of $\mathrm{ACI_N}$ is low with 0.10. Again, information on upward and downward motions were not taken into account in the data analysis.

**The large scatter in the observational data is a common feature in all publications dealing with aerosol-cloud interaction, discussed in section 4, and may partly reflect the technical/methodological difficulty to determine the true response of a given cloud layer to a given aerosol burden. Furthermore, young cloud layers, which just developed and are closely linked to the available aerosol particle concentration, as well as aged altocumulus layers, which may no longer be directly influenced by the found aerosol load, are typically probed. Uncertainties in the retrieved cloud properties (effective radius, CDNC, Table 1) and the fact that the particle extinction coefficient $\alpha_\mathrm{p}$ provides only estimates for the CCN concentration (aerosol particles with radii of roughly $50\,\mathrm{nm}$ and larger) contribute also to the large scatter in the found correlation between cloud and aerosol parameters in Fig. 3. The fact that vertical-wind information was not available in the majority of published studies, is the third and probably most important source for the large scatter in the correlation of aerosol and cloud properties and correspondingly low $\mathrm{ACI_N}$ values, as will be discussed in Sect. 3.3.**

Figure 4 presents the cloud-aerosol data sets for the cloud layer from the lowest occuring cloud base to $30\,\mathrm{m}$ above this lowest cloud base (see Fig. 1Figure 1) and for the layer from 70–$120\,\mathrm{m}$ above lowest cloud base. Together with Fig. 3 (cloud layer from 30–$70\,\mathrm{m}$ above cloud base) the results show the decreasing strength of the observed aerosol-cloud interaction with height above cloud base. Schmidt et al. (2013) stated that lidar observations at cloud base have to be exercised with caution because small variations in the cloud base height may lead to an inclusion of cloud free air in the cloud retrievals and may introduce a bias. Disregarding this potential bias, the aerosol-cloud interaction effect is small-

est in the cloud layer from 70–120 m with $ACI_N = 0$ and strongest just above cloud base ($ACI_N = 0.38$). Turbulent vertical mixing and entrainment of cloud-free and drier air from above probably weakened the aerosol effect on CDNC in the upper part of the shallow cloud layers. Entrainment of dry air may lead to a strong reduction of CDNC (evaporation of small droplets) and may significantly change the cloud droplet size distribution by collison and coagulation of droplets of different sizes in the upper cloud parts, and thus the droplet effective radii as discussed by Kim et al. (2008).

The dependence of $ACI_N$ on height above cloud base (laser penetration depth) as shown in Figs. 3 and 4 is summarized in Fig. 5 (green bars). The corresponding coefficients of determination for $ACI_N$ are compared in Fig. 6 to corroborate the statistical significance of our findings. The coefficients of determination show a strong decrease from the penetration depth of 30–70 m to 70–120 m.

### 3.3 $ACI_N$ during updraft periods

The main goal of Fig. 5, however, is to demonstrate the necessity to include vertical-wind information in ACI studies in layered clouds to obtain the most direct impact of aerosol particles on cloud microphysical properties. We contrast the results discussed before with our findings when vertical wind information, i.e., the knowledge on the occurrence of updrafts, is explicitly taken into account in the lidar signal averaging procedures. In the case of the red bars in Fig. 5, the basic lidar signal average profiles exclusively consider lidar returns measured during periods with positive vertical-wind component (>0 m/s at cloud base). Several examples showing the strong influence of the vertical air motion on cloud properties and aerosol-cloud interactions were discussed in Schmidt et al. (2014). Unfortunately, the number of co-located dual-FOV and Doppler lidar observations is about 50 % lower than the number of measured cloud cases with the dual-FOV Raman lidar alone. 13 cases of combined dual-FOV and Doppler wind lidar observations could finally be used for the calculation of the ACI values in Fig. 5 (red bars).

**As can be seen, $ACI_N$ is strongly increased for the updraft periods at all three height levels within the lowest 120 m of the altocumulus layers. Obviously a well-defined flow of CCN into clouds occurs during the updraft periods. A large decrease of $ACI_N$ is found again with increasing height above cloud base in these stratiform free-tropospheric cloud layers.**

**We cannot exclude that the observed aerosol-cloud correlation, which decreases with height, is partly linked to the fact that the Doppler-lidar-derived vertical-wind values at cloud base, used to separate upward and downward regions throughout the cloud layer, may not adequately represent the vertical-wind structures higher up in the altocumulus layers, so that lidar signal averaging (for updraft periods at cloud base) may include even downward moving cloud parcels, e.g., in the 70–120 m layer. This would partly smooth out the clear updraft effect in the cloud region from 70–120 m above cloud base.**

However, in the cloud layer from 30–70 m above cloud base, the $ACI_N$ value for updraft regions is $0.78 \pm 0.36$ and thus a factor of two larger than the corresponding $ACI_N$ value derived without consideration of the vertical wind velocity. The good correlation between the aerosol proxy and CDNC during updraft periods is corroborated by Fig. 6. The corresponding coefficient of determination reaches almost a value of 0.3 which is about a factor of three larger than the value derived without consideration of the vertical wind velocity.

For the updraft periods, $ACI_N$ is lower in the lowest 30 m above cloud base compared to the values for the 30–70 m cloud layer. Furthermore, the corresponding coefficient of determination is lower for the lowest 30 m of the cloud than for the 30–70 m layer. The results for the lowest 30 m of the clouds are probably affected by variations of the cloud base height (during the updraft periods). As mentioned, the trend that $ACI_N$ decreases with increasing height above cloud base (30-70 m versus 30–120 m height range) is consistent with the hypothsies that downdrafts, turbulent mixing, and entrainment processes immediately begin to reduce any clear aerosol effect on cloud microphysical properties on the way up through the cloud (Kim et al., 2008).

### 3.4 Discussion

**We found a clear indication that updraft knowledge is important for a realistic estimation of aerosol-cloud interaction. For all three defined cloud levels we observed a systematic increase of $ACI_N$ by 0.16-0.36, compared to the $ACI_N$ values when wind information is ignored. For the 30-70 m cloud layer, the standard deviation decreased from about 0.6 (for 26 cloud cases, green bars in Fig. 5) to 0.45 (for the 13 cloud layers, red bars). We may conclude that the standard deviation reduces by roughly a factor of 2 when updraft information is included in the analysis and the same number of clouds (e.g., 26) would have been available for statistical comparison. It is likely that the importance of updraft information in $ACI_N$ studies further increases if our sampled cloud data set would have been large enough to introduce even vertical-wind thresholds (not >0 m/s as considered in our study, but >0.5 m/s or 1 m/s) in the lidar signal averaging procedure. This aspect is discussed in the Sect. 4.2. A further reduction of the standard deviation of the found $ACI_N$ values (below 30%) is practically impossible because of the always remaining basic uncertainties in the lidar-derived aerosol and cloud parameters, as discussed above and summarized in Table 1.**

We may further conclude from the found importance of the updraft effect that any airborne study of aerosol-cloud interaction will significantly underestimate the true aerosol impact on CDNC if information on updraft and downdraft mo-

tion is not available and the research flight is not performed close to cloud base. This aspect (bias in airborne ACI studies) is further discussed in Sect. 4.

**In the case of satellite remote sensing with horizontal resolutions of kilometers so that updraft and downdraft regions cannot be resolved, $ACI_N$ must be generally interpreted with care. Even if the horizontal resolution would be high (a few 100 m) in satellite retrievals, the fact that most cloud information is related to cloud top areas and that vertical wind observations directly below the cloud are not available in the case of satellite remote sensing, will generally prohibit an accurate determination of $ACI_N$ from space.**

## 4 Literature review

We checked the literature concerning field studies of aerosol-cloud interactions of warm clouds of the past two decades for available ACI numbers. Main motivation was to answer the question how well our results are in agreement with other findings and what are the consequences in the ACI studies when vertical wind information is not available or not taken into account. Figure 7 summarizes this survey and may be regarded as an update of former efforts of ACI compilations (Twohy et al., 2005; Lu et al., 2008; McComiskey and Feingold, 2008, 2012). **However, such an extended overview as in Figure 7 has not been presented before, and permits a clear comparison of the impact of the different approaches (passive satellite remote sensing vs airborne retrievals vs ground-based attempts) on the ACI study results.** In the majority of considered satellite observations (red bars in Fig. 7) and airborne measurements (blue bars in Fig. 7), maritime layered clouds were investigated. With few exceptions, vertical wind information was not available or not considered in the measurements and retrievals shown in Fig. 7. As can be seen, almost the full range of physically meaningful $ACI_N$ values from 0 (no aerosol influence) to 1 (linear increase of CDNC with aerosol burden) is covered by observations. Even values $> 1$ are reported.

### 4.1 $ACI_N$ from satellite remote sensing

The wide spread of derived ACI values reflects first of all the use of different platforms (ground-based, airborne, spaceborne) and methods (different combinations of in situ measurements, active remote sensing, and passive remote sensing). As discussed in detail by McComiskey and Feingold (2012), the main reason for the relatively low $ACI_N$ values obtained from satellite passive remote sensing is that the analysis scale is in strong disagreement with the process scale. Aerosols influence cloud properties at the microphysical scale (process scale), but observations are most made of bulk properties over a wide range of resolutions (analysis scales). The most accurate representation of a process results from an analysis in which the process scale and analysis scale are the same. Typical cloud scales of variability (process scales, 100–1000 $\mathrm{m}$) are much smaller than the scales of variability in the aerosol properties (10–100 $\mathrm{km}$). Considering scales that drive convection, spatial scales of 10 to 100 m adequately capture bulk cloud properties. These small scales of variability may be observable from in situ and ground-based measurements but typically not from space, McComiskey and Feingold (2012) concluded.

Furthermore, radiation scattered by cloud edges can brighten the aerosol fields around clouds and can in this way systematically disturb the retrieval of aerosol optical depth and cloud properties used in satellite-based passive remote sensing ACI studies. Particle water-uptake in the aerosol layers around the clouds and lofted aerosol layers above the clouds (Painemal et al., 2014) are further sources of errors in the ACI studies from space. Aerosols detected and quantified around the cloud fields may not represent the desired aerosol conditions below cloud base.

Ma et al. (2014) recently reassessed the satellite data analysis presented in Quaas et al. (2008) (both papers are considered in Fig. 7) and included a longer time period. As a global average for cloud fields over the oceans, they found an $ACI_N$ value close to 0.4 from their state-of-the-art satellite observations. The study of Ma et al. (2014) offers the opportunity to discuss differences between ACI studies over continents (as our study) and oceans (most studies in Fig. 7). In contrast to the global mean $ACI_N$ value close to 0.4 over the oceans, they derived a global average $ACI_N$ value in the range of 0.1–0.15 over the continents (not shown in Fig. 7). The reason for the strong contrast between the $ACI_N$ values for clouds over land and sea may be related to the fact that the observed cloud fields over oceans form at comparably simple meteorological and aerosol conditions. The studied short-lived cumuli fields or aged stratocumulus layers mostly develop within a well-mixed, undisturbed marine boundary layer at almost adiabatic-like stratification of the water content resulting in an height-independent CDNC from cloud base to top (Painemal and Zuidema, 2013). Effects of vertical motions (updrafts, turbulent mixing, and entrainment of drier air into the clouds) may then be comparably weak (Twohy et al., 2005; Terai et al., 2012; Werner et al., 2014). In contrast, over land much more complex aerosol conditions (layering, spatial and temporal variability, composition, size distributions, mixtures of different aerosol types) prevail. Furthermore, the daily development of the boundary layer and nocturnal evolution of the residual layer lead to permanent changes in the updraft/downdraft characteristics (strengths, spatial distribution) in the lower troposphere up to several kilometers height. Orographic effects continuously disturb the air flow and may trigger gravity waves (and thus vertical motions) which influence cloud formation and microphysical properties in a complicated way. Over continents, vertical motions may thus play a much stronger role in cloud processes and may lead to a much stronger bias in the

ACI characterization if not considered.

### 4.2 $ACI_N$ from airborne observations

In strong contrast to the findings from spaceborne remote sensing, the majority of airborne observations lead to $ACI_N$ values of mostly $> 0.6$, as can be seen in Fig. 7. Most of these studies deal with shallow marine boundary-layer clouds (stratocumulus fields, convective cumuli) and consider the accumulation mode particle number concentration, i.e., aerosol particles with diameters larger than 80–100 nm, which best represent the CCN fraction. Cloud microphysical information from cloud base to top was used in most ACI analyses. Vertical motion was usually not taken into consideration.

However, several attempts are available in which the sensitivity of the ACI values on vertical motion was illuminated. McComiskey et al. (2009) investigated coastal stratiform clouds in California and found an increase of the mean $ACI_N$ value from 0.48 to 0.58 (for updraft periods with vertical winds $> 0.5\,\mathrm{ms}^{-1}$) and 0.69 (for periods with vertical winds $> 1\,\mathrm{ms}^{-1}$). McFarquhar and Heymsfield (2001) investigated aerosol-cloud relationships over the Indian Ocean and found only a slight increase in the mean $ACI_N$ values from 0.63 to 0.67 and 0.7 for data sets, considering only data for which the vertical winds were $< 0.5$, $> 0.5$–2, and $> 2\,\mathrm{ms}^{-1}$ in tropical cloud layers, respectively. Werner et al. (2014) found that updraft velocity variations from 0.5 to $4\,\mathrm{ms}^{-1}$ caused variations in the derived $ACI_r$ values by 0.02, or in terms of $ACI_N$ by 0.06. They concluded that updraft velocity strength is of minor importance in aerosol-cloud interaction studies of short-lived tropical trade wind cumuli over the tropical Atlantic. However, it is also interesting to note that Lu et al. (2008) found that better regression between maritime cloud and aerosol parameters is obtained when CDNC, accumulation mode particle number concentration $N_{\mathrm{acc}}$ and vertical velocity is considered in the regression study. The CDNC/$N_{\mathrm{acc}}$ ratio increased by about 30 % for updraft speeds around $2\,\mathrm{m\ s}^{-1}$ compared to the CDNC/$N_{\mathrm{acc}}$ ratio for a vertical velocity of $0.5\,\mathrm{m\ s}^{-1}$.

An interesting approach (leading to a high study-mean ACI of 0.86) is presented by Painemal and Zuidema (2013). They combined airborne fast (1 Hz sampling) in situ measurements of $N_{\mathrm{acc}}$ below the cloud with cloud optical depth and liquid water path values obtained from simultaneous observations (also at 1 Hz resolution) with upward-looking broadband irradiance and narrow field-of-view millimeter-wave radiometers. The authors argued that this approach works well over the oceans (in the boundary layer) when the cloud structure is well described by adiabatic conditions and a correspondingly height-independent CDNC profile, but may not work over continents with the mentioned complex cloud processes, aerosol mixtures, and varying vertical-wind conditions.

The maximum values of $ACI_N$ close to 1.05 in Fig. 7 are obtained from helicopter-borne observations of tropical, short-lived trade-wind cumuli around Barbados (Werner et al., 2014; Ditas, 2014). Werner et al. (2014) used two stacked payloads which were attached on top of each other to a helicopter by means of a 160 m long rope to perform in situ measurements within and collocated radiation measurements above clouds, 140 m above the in-situ aerosol and cloud observational platform which was attached to the end of the rope. The helicopter was moving with a comparably low horizontal speed of 15–20 $\mathrm{ms}^{-1}$. The observed clouds had horizontal extensions from 300–3000 m. The aerosol information for the ACI studies was taken from measurements in the subcloud layer (from the surface up to 400 m height), before the cloud observations were performed. As aerosol proxy they used the aerosol particles number concentrations considering particles with diameter $> 80$ nm only. Daily mean cloud effective radii (from the radiation measurements above the cloud) were combined with daily mean aerosol concentrations, measured in November 2010 and April 2011. Werner et al. (2014) found high $ACI_r$ around 0.35 (i.e., $ACI_N$ around 1.05) from these aerosol and cloud observations.

Ditas (2014) used the same cloud cases, but an alternative approach to study ACI. Only updraft periods were used in these ACI studies. The aerosol particle concentration outside of clouds was compared with the aerosol particle number concentrations inside the cloud layer. The difference between the two aerosol number concentrations was then interpreted as the activated particle number concentration (and taken as a proxy for CDNC) in the ACI studies. This approach is corroborated by a study of Zheng et al. (2011) in which a clear and strong dependence between measured CCN (for a relative humidity of 100.2 %) and CDNC was observed over the Pacific west of Chile.

### 4.3 $ACI_N$ from ground-based observations

Figure 7 also includes $ACI_N$ values (from 0.25 to 0.5) obtained from ground-based observations (green bars in Fig. 7) when combining aerosol data measured at the surface or at low heights with mostly column-integrated cloud properties which were retrieved from radiometer observations or from combined cloud radar and radiometer observations. These studies include clouds (convective and stratiform clouds) developing over land. The combination of surface aerosol information and remotely sensed cloud properties (mean values from base to top) is obviously only a rough approach (at least over land) to identify an impact of given aerosol conditions on cloud evolution and resulting properties for the reasons discussed above. Furthermore, $ACI_N$ values in Fig. 7 reported by Feingold et al. (2003) and McComiskey et al. (2009) are based on total aerosol particle number concentration, which include size ranges that are below the activation

diameter for cloud droplets (Werner et al., 2014). This fact also reduces the calculated ACI values.

**Finally, we include our own observations (orange bar in Fig. 7). The ACI value is taken from Fig. 5 (red bar for the 30–70 m layer) and considers the detailed information on particle extinction below cloud base, CDNC just above cloud base, and updraft periods in the data analysis. Our observations (over land) fit well with the airborne retrievals which were performed ovr the oceans.**

### 4.4 Literatur review: conclusions

In summary, we may conclude from Fig. 7 that all CCN become activated at cloud base when injected into the cloud from below, and correspondingly that $ACI_N$ is close to 1.0 at cloud base, disregarding whether the clouds are over the ocean or over continents. We can conclude that observations (and data analysis methods) yielding $ACI_N$ numbers far below 1, i.e. $< 0.5$, must at least be interpreted with care. In agreement with the extended discussion in the literature, it is obvious that satellite observations, focusing on ACI (with values mainly below 0.4), may not be appropriate to guide climate modelling activities (Quaas et al., 2009; Ban-Weiss et al., 2014; Ma et al., 2014).

## 5 Conclusions

Twenty nine cases of liquid-water cloud systems were observed with a novel dual-FOV Raman lidar over the polluted central European site of Leipzig, Germany, between September 2010 and September 2012. A collocated Doppler lidar was employed to provide measurements of up and downward motions at cloud base. The key results of the statistical analysis were presented and showed a clear aerosol signature on cloud evolution and CDNC in the lowest part of altocumulus layers during updraft periods with $ACI_N$. The comparison of the retrieved $ACI_N$ values showed good agreement with published aircraft observations of ACI, but also that passive satellite remote sensing delivers much lower $ACI_N$ values in comparison to our lidar and the airborne observations.

Because of the complex and combined influences of meteorological and aerosol-related aspects on cloud evolution and lifetime, strong efforts regarding field observations (in networks and in the framework of extended field campaigns) of aerosol and cloud properties and vertical velocity are requested. Measurements over the continents in polluted as well as pristine environments, covering all cloud types (convective and stratiform cloud systems) are required in order to improve our knowledge on the impact of man-made aerosols on cloud formation.

With respect to our own lidar approach we may conclude that the feasibilty study was successful and bears an exciting potential for cloud studies. However, to sample a necessary huge amount of cloud layers, the dual-FOV lidar must be upgraded in that way that automated observations around the clock are possible. We may thus think about to built a small compact automated lidar only with the dual-FOV option (two 607 Raman channels) and two polarization-sensitive 532 nm elastic-backscatter channels (to identify mixed-phase clouds) and to run this lidar together with an automated smart wind Doppler lidar over years.

*Acknowledgements.* The presented work was facilitated by the support of the whole group for ground-based remote sensing of the TROPOS institute. Fruitful discussions with Florian Ditas contributed to the work. The research leading to these results has received funding from the European Union Seventh Framework Programme (FP7/2007-2013) under grant agreement n 262254 (Aerosols, Clouds, and Trace gases Research Infrastructure Network, ACTRIS).

## References

Ansmann, A., Tesche, M., Seifert, P., Althausen, D., Engelmann, R., Fruntke, J., Wandinger, U., Mattis, I., and Müller, D.: Evolution of the ice phase in tropical altocumulus: SAMUM lidar observations over Cape Verde, J. Geophys. Res., 114, D17208, doi:10.1029/2008JD011659, 2009.

Ansmann, A., Fruntke, J., and Engelmann, R.: Updraft and downdraft characterization with Doppler lidar: cloud-free versus cumuli-topped mixed layer, Atmos. Chem. Phys., 10, 7845–7858, doi:10.5194/acp-10-7845-2010, 2010.

Ban-Weiss, G. A., Jin, L., Bauer, S. E., Bennartz, R., Liu, X., Zhang, K., Ming, Y., Guo, H., and Jiang, J. H.: Evaluating clouds, aerosols, and their interactions in three global climate models using satellite simulators and observations, J. Geophys. Res.-Atmos., 119, 10876–10901, doi:10.1002/2014JD021722, 2014.

Bréon, F., Tanré, D., and Generoso, S.: Aerosol effect on cloud droplet size monitored from satellite, Science, 295, 834–838, doi:10.1126/science.1066434, 2002.

Bühl, J., Ansmann, A., Seifert, P., Baars, H., and Engelmann, R.: Toward a quantitative characterization of heterogeneous ice formation with lidar/radar: comparison of CALIPSO/CloudSat with ground-based observations, Geophys. Res. Lett., 40, 4404–4408, doi:10.1002/grl.50792, 2013.

Bulgin, C. E., Palmer, P. I., Thomas, G. E., Arnold, C. P. G., Campmany, E., Carboni, E., Grainger, R. G., Poulsen, C., Siddans, R., and Lawrence, B. N.: Regional and seasonal variations of the Twomey indirect effect as observed by the ATSR-2 satellite instrument, Geophys. Res. Lett., 35, L02811, doi:10.1029/2007GL031394, 2008.

Costantino, L. and Bréon, F.-M.: Aerosol indirect effect on warm clouds over South-East Atlantic, from co-located MODIS and CALIPSO observations, Atmos. Chem. Phys., 13, 69–88, doi:10.5194/acp-13-69-2013, 2013.

Ditas, F.: Microphysical properties of aerosol particles in the trade wind regime and their influence on the number concentration of activated particles in trade wind cumulus clouds, Ph.D. thesis, University of Leipzig, Leipzig, 2014.

Engelmann, R., Wandinger, U., Ansmann, A., Müller, D., Zeromskis, E., Althausen, D., and Wehner, B.: Lidar observations of

the vertical aerosol flux in the planetary boundary layer, J. Atmos. Ocean. Tech., 25, 1296–1306, 2008.

Feingold, G., Remer, L., Ramaprasad, J., and Kaufman, Y.: Analysis of smoke impact on clouds in Brazilian biomass burning regions: an extension of Twomey's approach, J. Geophys. Res., 106, 22907–22922, doi:10.1029/2001JD000732, 2001.

Feingold, G., Eberhard, W. L., Veron, D. E., and Previdi, M.: First measurements of the Twomey indirect effect using ground-based remote sensors, Geophys. Res. Lett., 30, 1287, doi:10.1029/2002GL016633, 2003.

Feingold, G., Furrer, R., Pilewskie, P., Remer, L. A., Min, Q., and Jonsson, H.: Aerosol indirect effect studies at Southern Great Plains during the May 2003 Intensive Operations Period, J. Geophys. Res., 111, D05S14, doi:10.1029/2004JD005648, 2006.

Ferrare, R., Feingold, G., Ghan, S., Ogren, J., Schmid, B., Schwartz, S. E., and Sheridan, P.: Preface to special section: Atmospheric Radiation Measurement Program May 2003 Intensive Operations Period examining aerosol properties and radiative influences, J. Geophys. Res., 111, D05S01, doi:10.1029/2005JD006908, 2006.

Garrett, T. J., Zhao, C., Dong, X., Mace, G. G., and Hobbs, P. V.: Effects of varying aerosol regimes on low-level Arctic stratus, Geophys. Res. Lett., 31, L17105, doi:10.1029/2004GL019928, 2004.

Ghan, S. J., Chuang, C. C., and Penner, J. E.: A parameterization of cloud droplet nucelation, I, single aerosol type, Atmos. Res., 30, 197–211, 1993.

Ghan, S. J., Leung, L. R., Easter, R. C., and Abdul-Razzak, H.: Prediction of cloud droplet number in a general circulation model, J. Geophys. Res., 102, 21777–21794, doi:10.1029/97JD01810, 1997.

Ghan, S. J., Abdul-Razzak, H., Nenes, A., Ming, Y., Liu, X., Ovchinnikov, M., Shipway, B., Meskhidze, N., Xu, J., and Shi, X.: Droplet nucleation: physically-based parameterizations and comparative evaluation, J. Adv. Model. Earth Syst., 3, M10001, doi:10.1029/2011MS000074, 2011.

Gultepe, I., Isaac, G., Leaitch, W., and Banic, C.: Parameterizations of marine stratus microphysics based on in situ observations: implications for GCMs, J. Climate, 9, 345–357, doi:10.1175/1520-0442(1996)009<0345:POMSMB>2.0.CO;2, 1996.

Holben, B. N., Eck, T. F., Slutsker, I., Tanré, D., Buis, J. P., Setzer, A., Vermote, E., Reagan, J. A., Kaufman, Y. J., Nakajima, T., Lavenu, F., Jankowiak, I., and Smirnov, A.: AERONET – a federated instrument network and data archive for aerosol characterization, Remote Sens. Environ., 66, 1–16, 1998.

Illingworth, A. J., Hogan, R. J., O'Connor, E. J., Bouniol, D., Delanoe, J., Pelon, J., Protat, A., Brooks, M. E., Gaussiat, N., Wilson, D. R., Donovan, D. P., Klein Baltink, H., van Zadelhoff, G.-J., Eastment, J. D., Goddard, J. W. F., Wrench, C. L., Haeffelin, M., Krasnov, O. A., Russchenberg, H. W. J., Piriou, J.-M., Vinit, F., Seifert, A., Tompkins, A. M., and Willen. J., CLOUDNET: continuos evaluation of cloud profiles in seven operational models using ground-based observations, B. Am. Meteorol. Soc., 88, 883–898, 2007.

Kim, B.-G., Schwartz, S. E., and Miller, M. A.: Effective radius of cloud droplets by ground-based remote sensing: relationship to aerosol, J. Geophys. Res., 108, D23, doi:10.1029/2003JD003721, 2003.

Kim, B.-G., Miller, M. A., Schwartz, S. E., Liu, Y., and Min, Q.: The role of adiabaticity in the aerosol first indirect effect, J. Geophys. Res., 113, D05210, doi:10.1029/2007JD008961, 2008.

Lu, M.-L., Conant, W. C., Jonsson, H. H., Varutbangkul, V., Flagan, R. C., and Seinfeld, J. H.: The marine stratus/stratocumulus experiment (MASE): aerosol-cloud relationship in marine stratocumulus, J. Geophys. Res., 112, D10209, doi:10.1029/2006JD007985, 2007.

Lu, M.-L., Feingold, G., Jonsson, H. H., Chuang, P. Y., Gates, H., Flagan, R. C., and Seinfeld, J. H.: Aerosol-cloud relationships in continental shallow cumulus, J. Geophys. Res., 113, D15201, doi:10.1029/2007JD009354, 2008.

Ma, X., Yu, F., and Quaas, J.: Reassessment of satellite-based estimate of aerosol climate forcing, J. Geophys. Res. Atmos., 119, 10394–10409, doi:10.1002/2014JD021670, 2014.

Martin, G. M., Johnson, D. W., and Spice, A.: The measurement and parameterization of effective radius of droplets in warm stratocumulus clouds, J. Atmos. Sci., 51, 1823–1842, doi:10.1175/1520-0469(1994)051<1823:TMAPOE>2.0.CO;2, 1994.

Mattis, I., Ansmann, A., Müller, D., Wandinger, U., and Althausen, D.: Multiyear aerosol observations with dual-wavelength Raman lidar in the framework of EARLINET, J. Geophys. Res., 109, D13203, doi:10.1029/2004JD004600, 2004.

McComiskey, A. and Feingold, G.: Quantifying error in the radiative forcing of the first aerosol indirect effect, Geophys. Res. Lett., 35, L02810, doi:10.1029/2007GL032667, 2008.

McComiskey, A. and Feingold, G.: The scale problem in quantifying aerosol indirect effects, Atmos. Chem. Phys., 12, 1031–1049, doi:10.5194/acp-12-1031-2012, 2012.

McComiskey, A., Feingold, G., Frisch, A. S., Turner, D. D., Miller, M. A., Chiu, J. C., Min, Q., and Ogren, J. A.: An assessment of aerosol-cloud interactions in marine stratus clouds based on surface remote sensing, J. Geophys. Res., 114, D09203, doi:10.1029/2008JD011006, 2009.

Morales, R. and Nenes, A.: Characteristic updrafts for computing distribution-averaged cloud droplet number and stratocumulus cloud properties, J. Geophys. Res., 115, D18220, doi:10.1029/2009JD013233, 2010.

McFarquhar, G. and Heymsfield, A.: Parameterizations of INDOEX microphysical measurements and calculations of cloud susceptibility: applications for climate studies, J. Geophys. Res., 106, 28675–28698, doi:10.1029/2000JD900777, 2001.

Nakajima, T., Higurashi, A., Kawamoto, K., and Penner, J.: A possible correlation between satellite-derived cloud and aerosol microphysical parameters, Geophys. Res. Lett., 28, 1171–1174, doi:10.1029/2000GL012186, 2001.

O'Dowd, C., Lowe, J., Smith, M., and Kaye, A.: The relative importance of non-sea-salt sulphate and sea-salt aerosol to the marine cloud condensation nuclei population: an improved multi-component aerosol-cloud droplet parametrization, Q. J. Roy. Meteor. Soc., 125, 1295–1313, doi:10.1002/qj.1999.49712555610, 1999.

Painemal, D. and Zuidema, P.: The first aerosol indirect effect quantified through airborne remote sensing during VOCALS-REx, Atmos. Chem. Phys., 13, 917–931, doi:10.5194/acp-13-917-2013, 2013.

Painemal, D., Kato, S., and Minnis, P.: Boundary layer regulation in the southeast Atlantic cloud microphysics during

the biomass burning season as seen by the A-train satellite constellation, J. Geophys. Res.-Atmos., 119, 11288–11302, doi:10.1002/2014JD022182, 2014.

Pappalardo, G., Amodeo, A., Apituley, A., Comeron, A., Freudenthaler, V., Linné, H., Ansmann, A., Bösenberg, J., D'Amico, G., Mattis, I., Mona, L., Wandinger, U., Amiridis, V., Alados-Arboledas, L., Nicolae, D., and Wiegner, M.: EARLINET: towards an advanced sustainable European aerosol lidar network, Atmos. Meas. Tech., 7, 2389–2409, doi:10.5194/amt-7-2389-2014, 2014.

Quaas, J., Boucher, O., and Breon, F.: Aerosol indirect effects in POLDER satellite data and the Laboratoire de Meteorologie Dynamique-Zoom (LMDZ) general circulation model, J. Geophys. Res., 109, D08205, doi:10.1029/2003JD004317, 2004.

Quaas, J., Boucher, O., and Lohmann, U.: Constraining the total aerosol indirect effect in the LMDZ and ECHAM4 GCMs using MODIS satellite data, Atmos. Chem. Phys., 6, 947–955, doi:10.5194/acp-6-947-2006, 2006.

Quaas, J., Boucher, O., Bellouin, N., and Kinne, S.: Satellite-based estimate of the direct and indirect aerosol climate forcing, J. Geophys. Res., 113, D05204, doi:10.1029/2007JD008962, 2008.

Quaas, J., Ming, Y., Menon, S., Takemura, T., Wang, M., Penner, J. E., Gettelman, A., Lohmann, U., Bellouin, N., Boucher, O., Sayer, A. M., Thomas, G. E., McComiskey, A., Feingold, G., Hoose, C., Kristjánsson, J. E., Liu, X., Balkanski, Y., Donner, L. J., Ginoux, P. A., Stier, P., Grandey, B., Feichter, J., Sednev, I., Bauer, S. E., Koch, D., Grainger, R. G., Kirkevåg, A., Iversen, T., Seland, Ø., Easter, R., Ghan, S. J., Rasch, P. J., Morrison, H., Lamarque, J.-F., Iacono, M. J., Kinne, S., and Schulz, M.: Aerosol indirect effects – general circulation model intercomparison and evaluation with satellite data, Atmos. Chem. Phys., 9, 8697–8717, doi:10.5194/acp-9-8697-2009, 2009.

Raga, G. and Jonas, P.: On the link between cloud-top radiative properties and sub-cloud aerosol concentrations, Q. J. Roy. Meteor. Soc., 119, 1419–1425, doi:10.1002/qj.49711951410, 1993.

Ramanathan, V., Crutzen, P., Kiehl, J., and Rosenfeld, D.: Atmosphere – aerosols, climate, and the hydrological cycle, Science, 294, 2119–2124, doi:10.1126/Science.1064034, 2001.

Riihimaki, L. D., McFarlane, S. A., and Comstock, J. M.: Climatology and Formation of Tropical Midlevel Clouds at the Darwin ARM Site, J. Climate, 25, 68356850, doi:10.1175/JCLI-D-11-00599.1, 2012.

Schmidt, J.: Dual-field-of-view Raman lidar measurments of cloud microphysical properties – investigation of aerosol-cloud intercations, Ph.D. thesis, University of Leipzig, Leipzig, 2014.

Schmidt, J., Wandinger, U., and Malinka, A.: Dual-field-of-view Raman lidar measurments for the retrieval of cloud microphysical properties, Appl. Opt., 52, 2235–2247, 2013.

Schmidt, J., Ansmann, A., Bühl, J., Baars, H., Wandinger, U., Müller, D., and Malinka, A. V.: Dual-FOV Raman and Doppler lidar studies of aerosol-cloud interactions: simultaneous profiling of aerosols, warm-cloud properties, and vertical wind, J. Geophys. Res., 119, 5512–5527, doi:10.1002/2013JD020424, 2014.

Shupe, M. D.: A ground-based multisensor cloud phase classifier, Geophys. Res. Lett., 34, L22809, 10.1029/2007GL031008, 2007.

Sekiguchi, M., Nakajima, T., Suzuki, K., Kawamoto, K., Higurashi, A., Rosenfeld, D., Sano, I., and Mukai, S.: A study of the direct and indirect effects of aerosols using global satellite data sets of aerosol and cloud parameters, J. Geophys. Res., 108, 4699, doi:10.1029/2002JD003359, 2003.

Terai, C. R., Wood, R., Leon, D. C., and Zuidema, P.: Does precipitation susceptibility vary with increasing cloud thickness in marine stratocumulus?, Atmos. Chem. Phys., 12, 4567–4583, doi:10.5194/acp-12-4567-2012, 2012.

Twohy, C., Petters, M., Snider, J., Stevens, B., Tahnk, W., Wetzel, M., Russell, L., and Burnet, F.: Evaluation of the aerosol indirect effect in marine stratocumulus clouds: droplet number, size, liquid water path, and radiative impact, J. Geophys. Res., 110, D08203, doi:10.1029/2004JD005116, 2005.

Twomey, S. A.: The nuclei of natural cloud formation. Part II: the supersaturation in natural clouds amd variation of cloud droplet concentration, Geofis. Pura Appl., 43, 243–249, 1959.

Wandinger, U., Seifert, P., Wagner, J., Engelmann, R., Bühl, J., Schmidt, J., Heese, B., Baars, H., Hiebsch, A., Kanitz, T., Althausen, D., and Ansmann, A.: Integrated remote-sensing techniques to study aerosols, clouds, and their interaction, in: Proceedings, 26th International Laser Radar Conference, Volume I, Porto Heli, Greece, 25–29 June 2012, 395–398, 2012.

Werner, F., Ditas, F., Siebert, H., Simmel, M., Wehner, B., Pilewskie, P., Schmeissner, T., Shaw, R. A., Hartmann, S., Wex, H., Roberts, G. C., and Wendisch, M.: Twomey effect observed from collocated microphysical and remote sensing measurements over shallow cumulus, J. Geophys. Res.-Atmos., 119, 1534–1545, doi:10.1002/2013JD020131, 2014.

Zheng, X., Albrecht, B., Jonsson, H. H., Khelif, D., Feingold, G., Minnis, P., Ayers, K., Chuang, P., Donaher, S., Rossiter, D., Ghate, V., Ruiz-Plancarte, J., and Sun-Mack, S.: Observations of the boundary layer, cloud, and aerosol variability in the southeast Pacific near-coastal marine stratocumulus during VOCALS-REx, Atmos. Chem. Phys., 11, 9943–9959, doi:10.5194/acp-11-9943-2011, 2011.

**Table 1. Lidar parameters, signal sampling resolution and typical signal averaging periods (used in the retrieval of cloud products), the retrieved aerosol and cloud products, and respective uncertainties in the products. Absolute uncertainty in wind observation is 5–15 cm/s. Typical errors are given. Doppler lidar and dual-FOV Raman lidar were located within a distance of less than 10 m and both lidars were pointing exactly to the zenith.**

| Lidar | Signal, vertical and temporal resolution | Product, vertical and temporal resolution | Product | Rel. uncertainty (signal noise) | Rel. uncertainty, (retrieval) |
|---|---|---|---|---|---|
| Doppler lidar | 2 s, 70 m | 10 s, 70 m | Vertical wind | 10–20% | 10–20% |
| Dual-FOV Raman lidar | 10 s, 15 m | 10–90 min, 30-50 m | Aerosol extinction coefficient | 5–10% | 10–20% |
| | | | Cloud extinction coefficient | 5–10% | 5-10% |
| | | | Cloud droplet effective radius | 10–15% | 15–25% |
| | | | Cloud droplet number conc. | | 25–75% |

**Table 2.** Aerosol and cloud properties of 29 studied aerosol-cloud scenarios. The range of observed aerosol extinction coefficients and cloud optical thicknesses and the corresponding mean values and standard deviations (SD) are given for 532 nm wavelength.

| | Range | Mean ($\pm$SD) |
|---|---|---|
| Aerosol extinct. coef. ($Mm^{-1}$) | 7–130 | $52 \pm 34$ |
| Cloud base height (m) | 1100–4400 | $2900 \pm 910$ |
| Cloud vertical extent (m) | 95–300 | $190 \pm 50$ |
| Cloud optical thickness | 1.5–5.9 | $3.6 \pm 1.3$ |
| LWP ($gm^2$) | 5.4–64 | $19 \pm 4$ |

**Table 3.** Statistics of cloud extinction coefficients (532 nm), droplet effective radii, LWCs, and CDNCs, derived from the dual-FOV Raman lidar observations. Range of values (minumum to maximum), mean values, and standard deviations (SD) are presented.

| | | Height range above cloud base | | |
|---|---|---|---|---|
| | | 0–30 m | 30–70 m | 70–120 m |
| Cloud extinction coefficient | Min ($km^{-1}$) | 2.6 | 3.9 | 5.1 |
| | Max ($km^{-1}$) | 28.3 | 36.3 | 44.4 |
| | Mean ($km^{-1}$) | 11.5 | 19.4 | 25.5 |
| | SD ($km^{-1}$) | 5.7 | 7.0 | 11.4 |
| Droplet effective radius | Min (µm) | 2.7 | 3.0 | 2.9 |
| | Max (µm) | 11.0 | 14.5 | 13.8 |
| | Mean (µm) | 5.8 | 9.0 | 10 |
| | SD (µm) | 1.9 | 3.0 | 2.6 |
| LWC | Min ($gm^{-3}$) | 0.010 | 0.012 | 0.020 |
| | Max ($gm^{-3}$) | 0.213 | 0.243 | 0.391 |
| | Mean ($gm^{-3}$) | 0.049 | 0.124 | 0.188 |
| | SD ($gm^{-3}$) | 0.041 | 0.063 | 0.102 |
| CDNC | Min ($cm^{-3}$) | 10 | 12 | 13 |
| | Max ($cm^{-3}$) | 460 | 545 | 496 |
| | Mean ($cm^{-3}$) | 112 | 92 | 72 |
| | SD ($cm^{-3}$) | 102 | 110 | 88 |

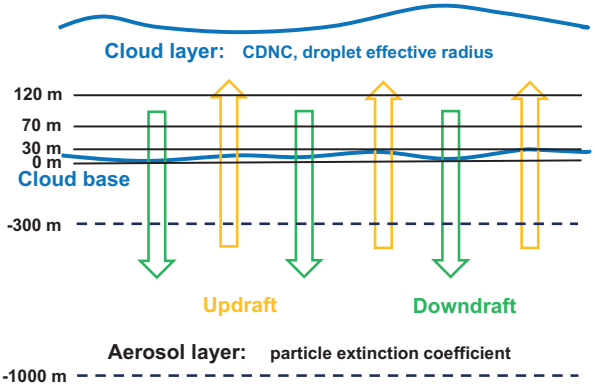


**Fig. 1. Sketch to illustrate our lidar-based approach to investigate aerosol-cloud interactions (ACI) in case of pure liquid-water clouds (blue lines indicate cloud bottom and top). The particle extinction coefficient measured with the Raman lidar in the height range from 300–1000 m below the lowest cloud base height (at 0 m in the sketch) is used as aerosol proxy (dashed lines indicate base and top of the considered aerosol layer). From the dual-FOV Raman lidar observations we determine the cloud droplet number concentration (CDNC) and the effective radius for cloud layers from the lowest occuring cloud base to 30 m above lowest cloud base, from 30–70 m, and from 70–120 m above the lowest cloud base. A collocated Doppler lidar measures the vertical wind component and thus periods with updraft and downdraft motions.**

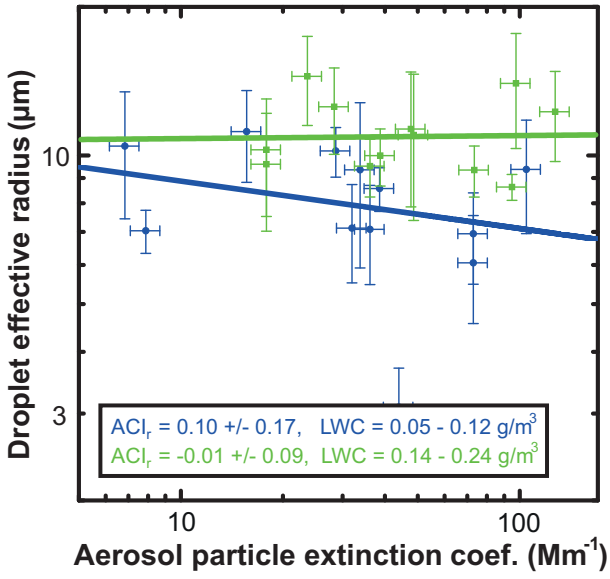


**Fig. 2.** Cloud droplet effective radius (mean value for the height range from 30–70 m above cloud base) vs. aerosol particle extinction coefficient (mean value for the layer from 300–1000 m below cloud base). 26 cloud cases are considered. The corresponding $ACI_r$ values (negative slopes of the green and blue lines) are given as numbers together with the standard deviations. The overall mean $ACI_r$ value is $0.04 \pm 0.09$. Vertical wind information is not considered in this analysis. Error bars show the uncertainties in the retrieved aerosol and cloud parameters. An error discussion is given in Schmidt et al. (2014).

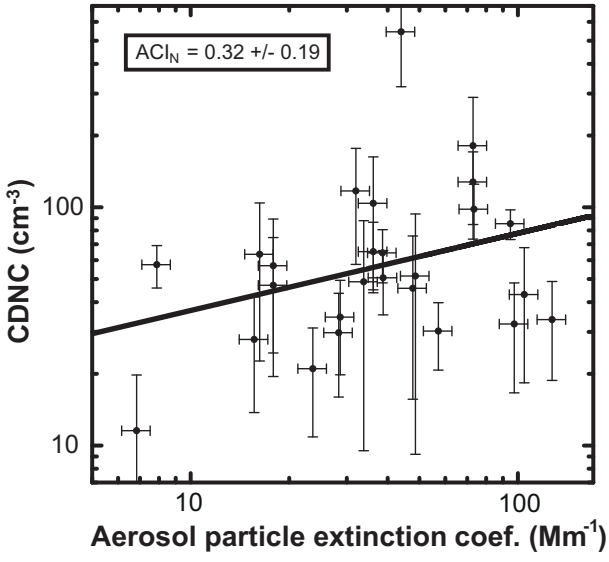


**Fig. 3.** Cloud droplet number concentration (CDNC, for the 30–70 m layer above cloud base) vs. aerosol particle extinction coefficient (mean value for the layer from 300–1000 m below cloud base) for 26 dual-FOV Raman lidar probings. The linear regression of the data yields $ACI_N = 0.32 \pm 0.19$ (slope of the black line). Information of up- and downdraft periods is not considered in this analysis. Error bars show the retrieval uncertainties.

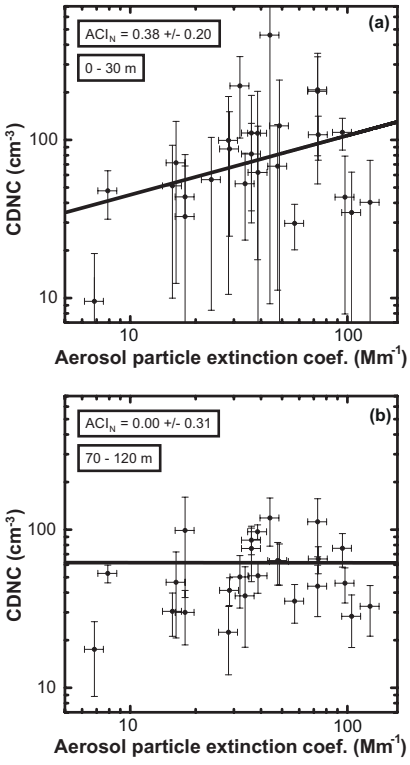


**Fig. 4.** Same as Fig. 3, except for cloud layers from **(a)** cloud base to 30 m above cloud base and **(b)** for the 70–120 m layer above cloud base. The corresponding mean $ACI_N$ value and SD are given as numbers.

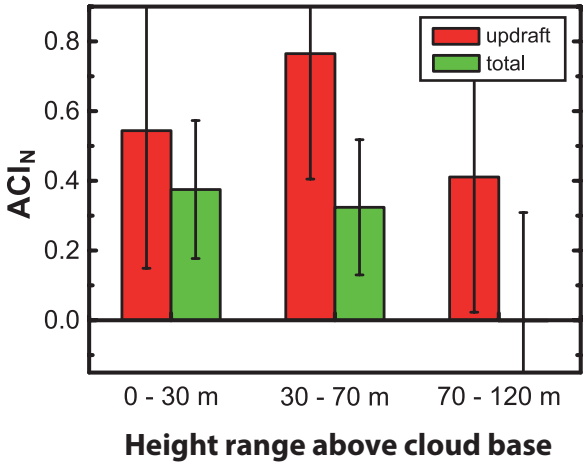


**Fig. 5.** $ACI_N$ for updraft periods only (red, 13 cases) and when vertical wind information is not taken into account in the lidar data analysis and ACI retrieval (green, 26 cases). Error bars show the overall variability caused by atmospheric variability and retrieval uncertainties.

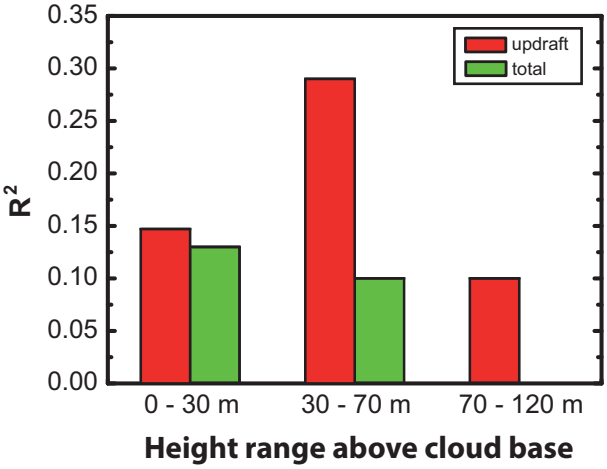


**Fig. 6.** Coefficient of determination $R^2$ in the case of linear regression of aerosol proxy and CDNC to obtain $ACI_N$ as shown in Figs. 3 and 4. The green bars show $R^2$ when vertical wind information is ignored. The red bars are obtained when data only for updraft periods are considered in the linear regression.

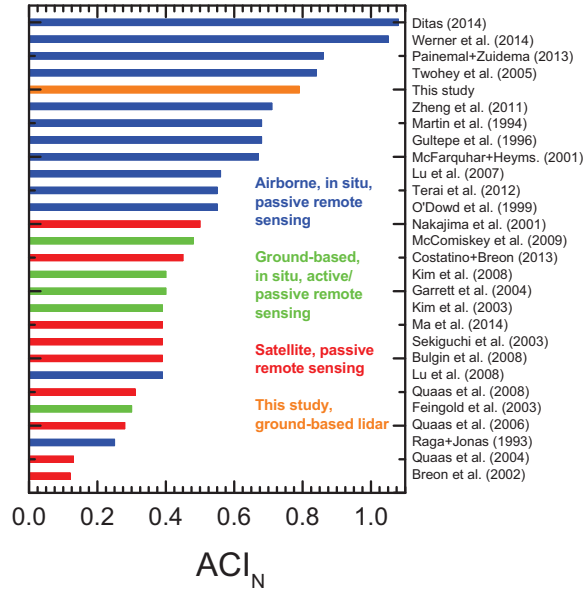


**Fig. 7.** $ACI_N$ values as published in the literature (see references to the right). Different methods (in situ measurements, remote sensing) and observational platforms (aircraft, satellite, ground-based) are used. The orange bar (this study) is taken from Fig. 5 (red bar, 30–70 m above cloud base).